Deep Mining 2024 – P Andrieux & D Cumming-Potvin (eds)

doi:10.36487/ACG_repo/2465_91

Insights from seismic analysis at Kiruna mine

Rebecca Westley-Hauta [a,*], Stephen Meyer [b], Phil Earl [c]

[a] *LKAB, Sweden*

[b] *Institute of Mine Seismology, Canada*

[c] *Global Mine Design, UK*

Abstract

Kiruna is a sublevel caving mine in Kiruna, Sweden that produced more than 25 million tonnes in 2023. As mining gets deeper at Kiruna mine, analysis of seismic data to understand the nature of seismic risks has become more critical and the mine has had to continue developing strategies that mitigate the impact of seismicity.

This paper will cover the evolving trends in mine seismicity since a large ML4.2 event in May 2020 resulted in changes to Kiruna's production strategy and the closure of many mining areas. This includes a description of the mine's seismic system and expansion plans, various quantitative analyses of the mine's seismicity and insight into the use of moment tensor decompositions to understand the source mechanisms of rock mass failures.

Keywords: *mine seismicity, seismic systems, source mechanisms*

1 Overview of Kiruna mine

1.1 Mine layout and mining method

The Kiruna iron ore mine operated by LKAB (Sweden) is one of the largest sublevel caving operations in the world and produces approximately 80% of Europe's iron ore (Lindberg 2023). Mining began in 1898 as an open pit operation. By the mid-1950s the mine began transitioning to underground mining and production has been fully underground since 1962. Significant seismicity issues emerged between 2007 and 2008 when mining activities reached a depth of approximately 670 m below the surface (Dineva & Boskovic 2017). As of 2024, mining takes place on levels 1022 to 1137 (approximately 800 to 900 m underground). Since its inception, the Kiruna mine has extracted over one billion tonnes of ore, with recent annual production shown in Figure 1.

Kiruna mine uses the sublevel caving mining method. The mine is subdivided into 10 mining blocks which are accompanied by orepasses (referred to as TG). Material is transported to crushing stations from the 1365 level, and then hoisted to the surface via a network of five internal winzes and eight shafts to the surface. A simplified version of the material handling system infrastructure is shown in Figure 2. Staggered blasting patterns are drilled upward and blasted in a retreat towards the footwall while respecting lead-lag guidelines in the horizontal and vertical directions. Kiruna has increased the sublevel spacing and distance between crosscuts over time and is currently mining in the dimensions shown in Figure 2.

* Corresponding author.

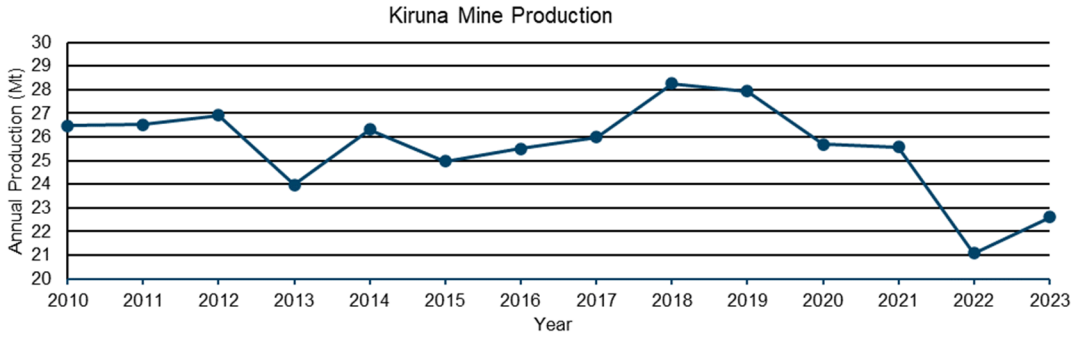

Figure 1 **Kiruna mine production from 2010 to 2023 (after McGurk et al. 2023). Note the production decrease after 2020, partly due to the large seismic event in May 2020**

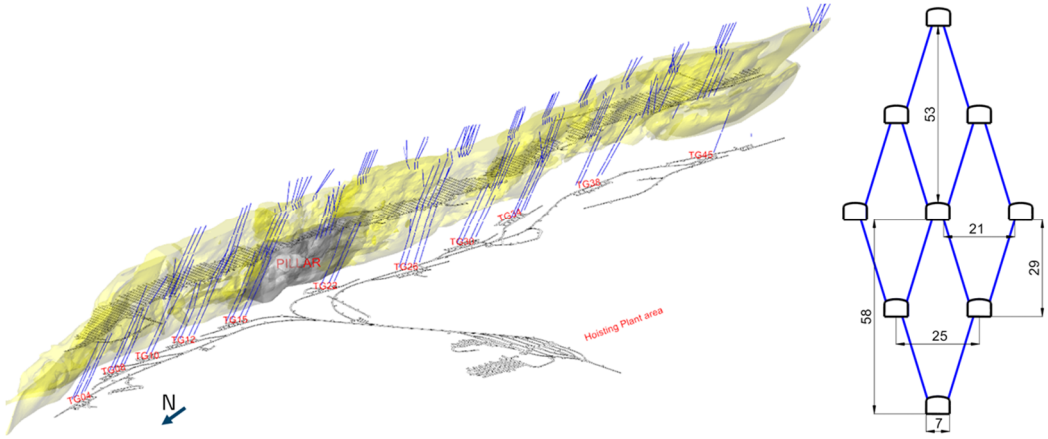

Figure 2 **(a) KUJ orebody with production level 1051, main level 1365 and orepass shown (McGurk et al. 2023); (b) Sublevel caving geometry used at Kiruna mine**

Blasting during the period of 1 November 2023 to 1 May 2024 on levels 1022–1137 is shown in plan view in Figure 3.

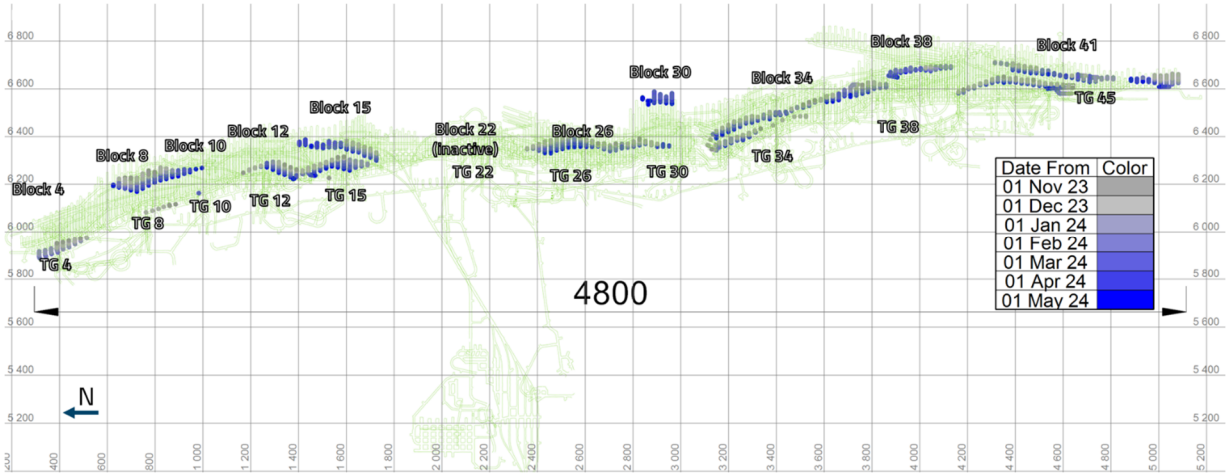

Figure 3 **Plan view of more than 1,600 blasts fired on levels 1022–1137 between 1 January to 1 May 2024, with blocks and orepass groups (TG) labelled**

1.2 Geology and rock mass

1.2.1 Mine geology

The Kiirunavaara orebody exploited by Kiruna mine is a tabular iron oxide-apatite deposit of the Paleoproterozoic age. It is over 4 km long, with thickness ranging from 0 to 200 m. It extends to at least 1,300 m below ground surface, strikes north to south, and dips between 50° and 60° to the east.

The orebody has been emplaced within a succession of metavolcanic rocks that lie unconformably over Archean basement and an early Paleoproterozoic rift-related volcano-sedimentary formation (Bergman et al. 2001; Martinsson 2004). The footwall-ore-hanging wall rock sequence is within the Kiirunavaara Group, with an age range believed to be between 1.90 to 1.87 giga annum (Ga) (Westhues et al. 2016; Allen 2021). The footwall rocks comprise mafic-intermediate volcanic units of the Hopukka formation, while the hanging wall consists of rhyolitic-rhyodacitic metavolcanic rocks of the Luossavaara formation. There are generally sharp contacts between the ore and host rock, although variable contacts do occur.

At the mine-scale, the mafic-intermediate volcanic footwall rocks are trachyandesite but are traditionally referred to as syenite porphyry (SP). SP units are subdivided according to properties, where SP1, SP2 and SP4 are grouped together as the least altered trachyandesites. SP1 is dark-coloured with very few feldspar phenocrysts, SP2 shows a blotchy alteration of silica-rich minerals and SP4 is dark-coloured with elongated plagioclase feldspar phenocrysts. SP3 is a nodular porphyry with distinctive reddish colouration and contains various mineral aggregates and inclusions of actinolite, apatite, magnetite, titanite and biotite. SP5 is a collective term for variously more altered footwall rocks; alteration is generally by lower strength minerals such as carbonates, sulphates, chlorite, talc, etc. (Andersson et al. 2021). Ore is subdivided into phosphorus-rich ore, phosphorus-poor ore and unlabelled ore. The rhyolitic-rhyodacitic metavolcanic hanging wall rocks were originally grouped as quartz-porphyry (Qp) due to a lack of detailed descriptions (Geijer 1910; Andersson et al. 2021). They generally comprise a more quartz-rich composition compared to the footwall rocks and may contain rounded phenocrysts of feldspar. Cutting across the orebody, near-perpendicular, are porphyry dykes traditionally referred to as dyke-porphyry (Dp) and similar in composition to the hanging wall Qp. In the deeper parts of the footwall (below 900 m) a red-coloured granite occurs: referred to as central facility granite (CA), it is mostly even-grained but can appear porphyritic and sometimes contains mafic enclaves (Andersson et al. 2012).

1.2.2 Intact rock strength

Intact rock strengths of key rock types were recently compiled from records dating between 1987 and 2019, with values summarised in Table 1. Much effort was placed on validating quality and grouping the data into the seven mine-scale rock unit categories, which serve as the basic rock units for numerical modelling and other mine-based studies (Andersson et al. 2021).

Table 1 Compilation of rock mass properties from Andersson et al. (2021)

Lithology	Ore	Qp	Sp 1,2,4	Sp 3	Sp 5	Dp	CA
# samples	103	99	61	39	14	11	10
Min (MPa)	52	52	157	91	60	201	242
Mean (MPa)	143	230	368	227	156	346	260
Max (MPa)	352	488	586	411	341	550	313
Std. dev (MPa)	53	104	109	81	89	108	55
Median (MPa)	144	220	373	225	123	343	275

1.2.3 Mechanical rock properties

Other mechanical properties are summarised in Table 2. These data are compiled from studies by Sjöberg et al. (2001) and were not included in the 2021 rock strength study. The 2021 study recommends adopting the lower-bound unconfined compressive strength (UCS) for SP5. Comparison of the other UCS values indicates with reasonable confidence that the 2001 mechanical property data remain appropriate for design use.

Table 2 Mechanical properties of key rock types (after Sjöberg et al. 2001)

Lithology	Ore	Qp	Sp 1,2,4	Sp 3	Sp 5	Dp	CA
Density (kg/m^3)	4,700	2,700	2,800	2,800	2,800	–	–
Young's modulus (GPa)	60–100	37–81	70	44–60	80	75	75
Poisson's ratio	0.18–0.28	0.14–0.27	0.2–0.27	0.14–0.24	–	–	–
Compressive strength (MPa)	133	184	300	210	430	90	320
Tensile strength (MPa)	10	12	10	11	10	–	–
Cohesion (MPa)	16–108	88–117					
Friction angle (°)	22–43	35–38					

Kiruna mine's database of geological strength index (GSI) estimations collected during geological mapping of new development rounds was used to graph the distribution of GSI in the rock mass (Figure 4).

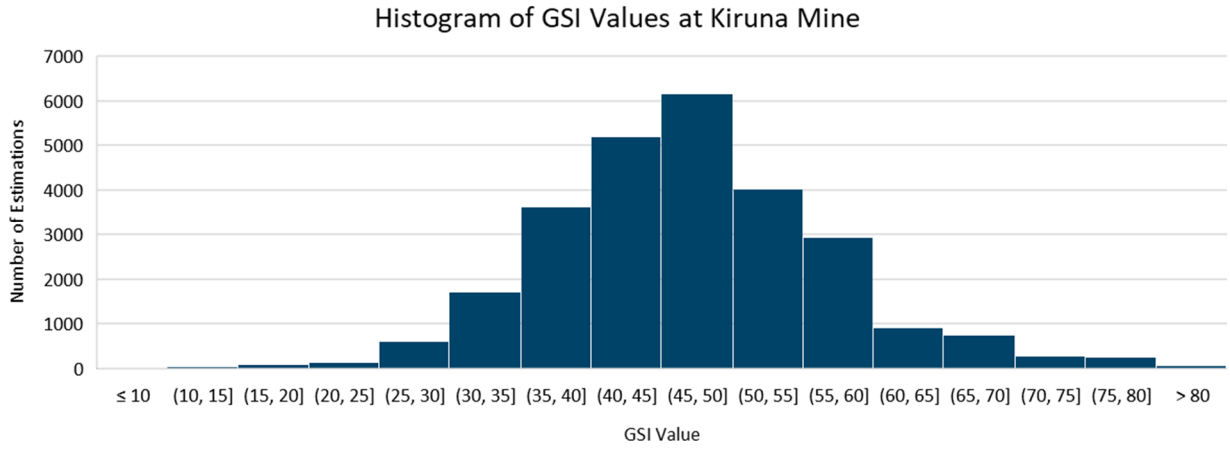

Figure 4 Geological strength index estimations from more than 26,000 observations in Kiruna mine's database

1.3 In situ stress

Kiruna stress data in literature is most commonly taken from studies by Sandström (2003), where:

- $\sigma_H = 7.7 + 0.037\ z$ – direction perpendicular to orebody strike
- $\sigma_h = 5.6 + 0.028\ z$ – direction subparallel to orebody strike
- $\sigma_v = 5.8 + 0.029\ z$ – direction sub-vertical with dip.

Between 2018 and 2020 an additional series of stress measurements were undertaken as part of studies relating to future mining at depth. The tests were a mixture of 10 m drillholes above existing drives and long drillholes up to 700 m below existing drillholes. The additional testing is summarised in Table 3.

Table 3 Summary of recent stress measurements

Year	Company	Method	Mine elevation and test locations
2018	Sigra	Over-coring	Approximately 2,045 mRL (deep borehole)
2018	SCT	Over-coring	1,395 mRL, 1,402 mRL, 1,684 mRL and 2,080 mRL (deep borehole)
2020	Golder	CSIRO hollow inclusion	Approximately 1,365 mRL (short borehole above drive)
2020	Stress measurement company	LVDT measurements	Approximately 1,365 mRL (short borehole above drive)

Stress magnitudes are depicted in Figure 5. The stress gradients are taken from Sandström (2003) and are extended only as far as existing development. Short drillhole data clustered around 1,400 mRL provide some confidence as to the precision of the historical stress gradients, although it is noted that σ_h and σ_v sometimes vary between σ_2 and σ_3, respectively. The long drillhole data shows an increase of σ_v with depth but σ_H and σ_h remain constant. Numerical model studies are currently underway that may provide more insight into stress conditions beneath mine development and the potential influence of the cave.

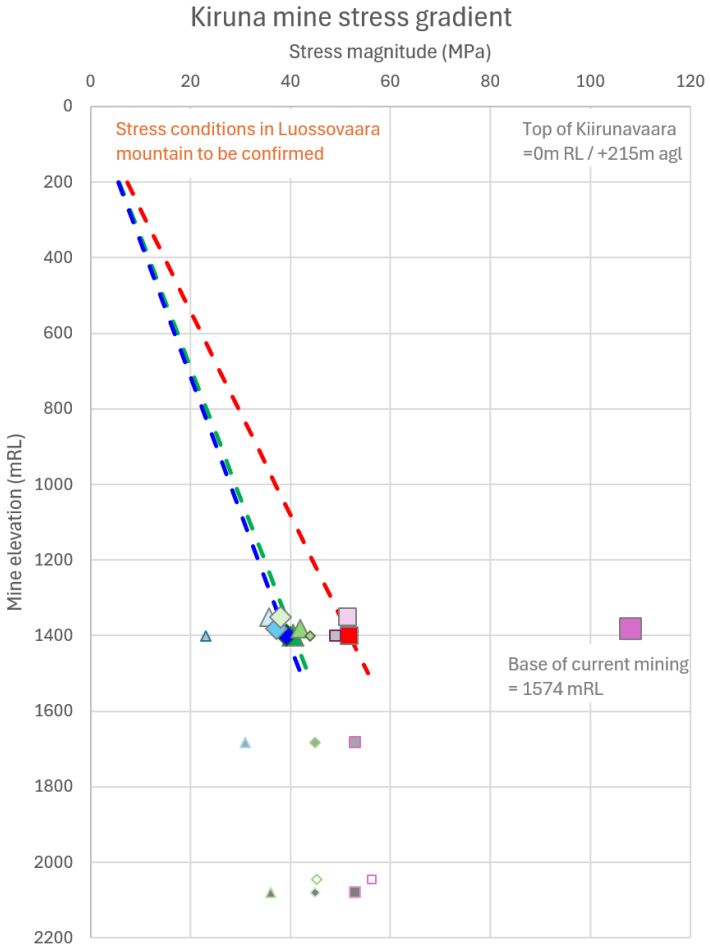

Figure 5 Current stress magnitude data with depth

1.4 Kiruna's seismic system and expansion plans

As of May 2024 the Kiruna seismic system comprises 76 stations with 123 uniaxial geophones, 121 triaxial geophones (14 and 4.5 Hz) and four triaxial strong ground motion MEMS accelerometers. A view looking east of the mine is shown in Figure 6 to illustrate the installed sensor array and the planned array expansion to be completed during 2024 and 2025.

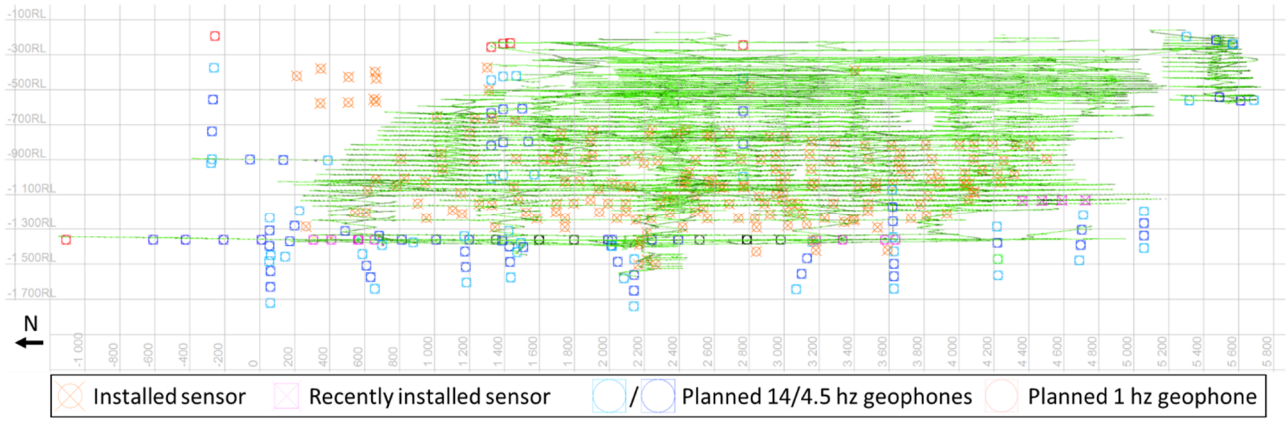

Figure 6 Current and planned sensor array expansion. Note that the satellite zone to the south is a smaller LKAB mine, Konsuln. The sensors installed in this mine will cover both Kiruna and Konsuln

2 ML4.2 event in May 2020

On 18 May 2020 a magnitude 4.2 event took place in the Block 22 sector of the mine. Damage mapping after this event revealed that at least 3 km of drifts had completely collapsed (R5, according to the rockburst damage scale by Heal et al. 2006; Kaiser et al. 1992), and more than 3 km had experienced R3 and R4 levels of damage. Damage zones are shown in Figure 7.

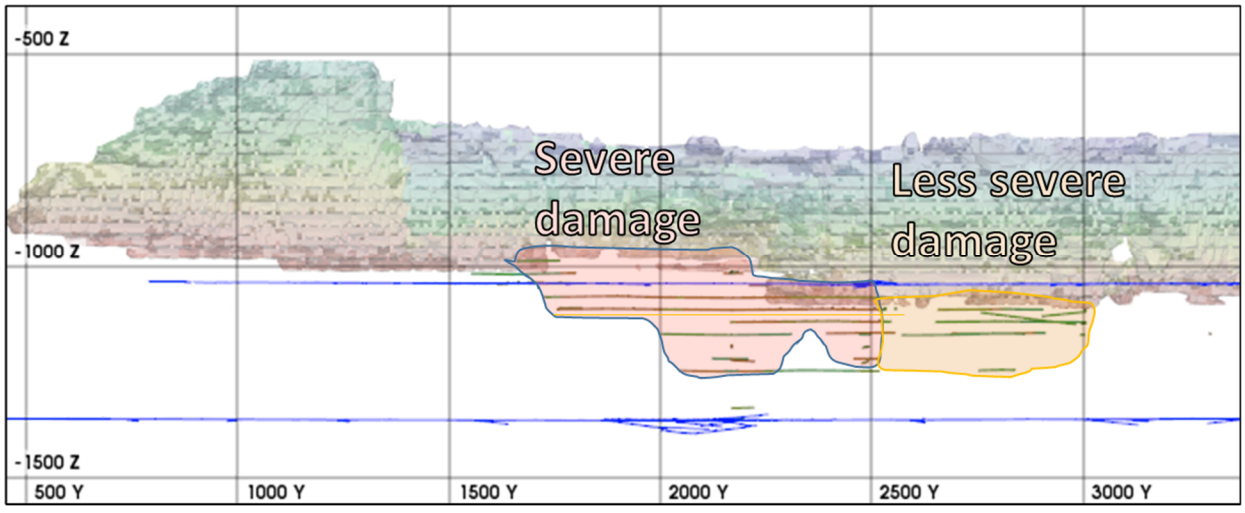

Figure 7 View looking east of damaged zones (after Swedberg 2022)

2.1 Overview of seismicity since the May 2020 event

Trends in seismicity in the direct vicinity of the source of the May 2020 large event (around Block 22, from 1,800 < south < 2,400) since then are shown in this section. Seismic source mechanisms are evaluated routinely at Kiruna, with 20% of all genuine events in 2023 having a source mechanism calculated. This allows investigation of the different failure modes of events in the mine and how they vary. Figure 8 compares the logP size distribution of slip- and crush-type sources in Block 22 since the May 2020 large event. It shows that at the larger end, slip- and crush-type events of around MW1.5 have been recorded. However, one also observes that there are more crush-type events with lager magnitudes and that crush-type events have a lower slope than slip-type. These findings are due to seismicity induced by sequencing at Kiruna and geometrical factors (Ylmefors 2023), which is in contrast to observations at many other mines.

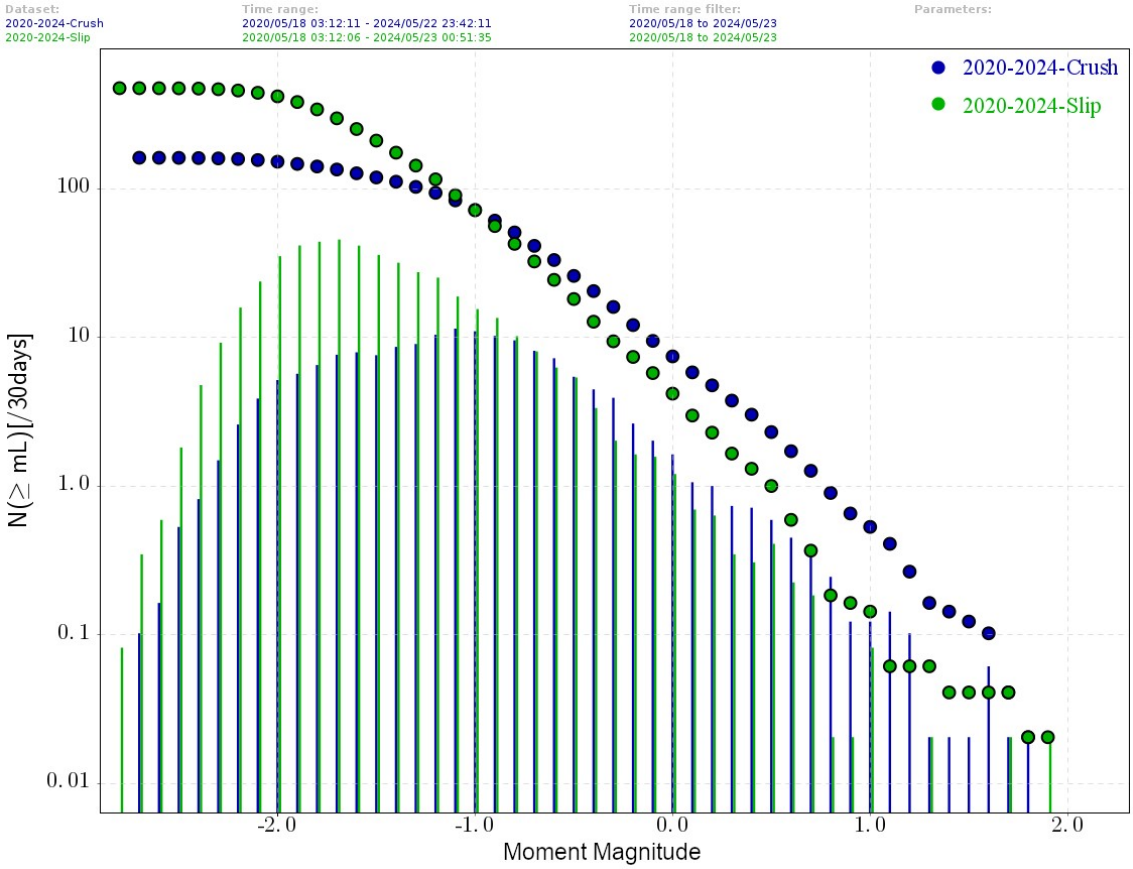

Figure 8 Size distribution plot of slip-type and crush-type events recorded between 1,800 < south < 2,400 in the production areas and footwall

Another observation is that, overall, there are more slip-type events, and that slip-type events seem to have a smaller MMIN. While the exact, true MMIN is not entirely evident as the change is gradual (likely due to variations in system coverage, mining and activity levels), the number of slip-type events observed seems to decrease around M=–2.0, while this turning point is notably higher for crush-type events, at around M=–1.0. This can likely be explained by the fact that slip-type events are more energetic, as illustrated in Figure 9.

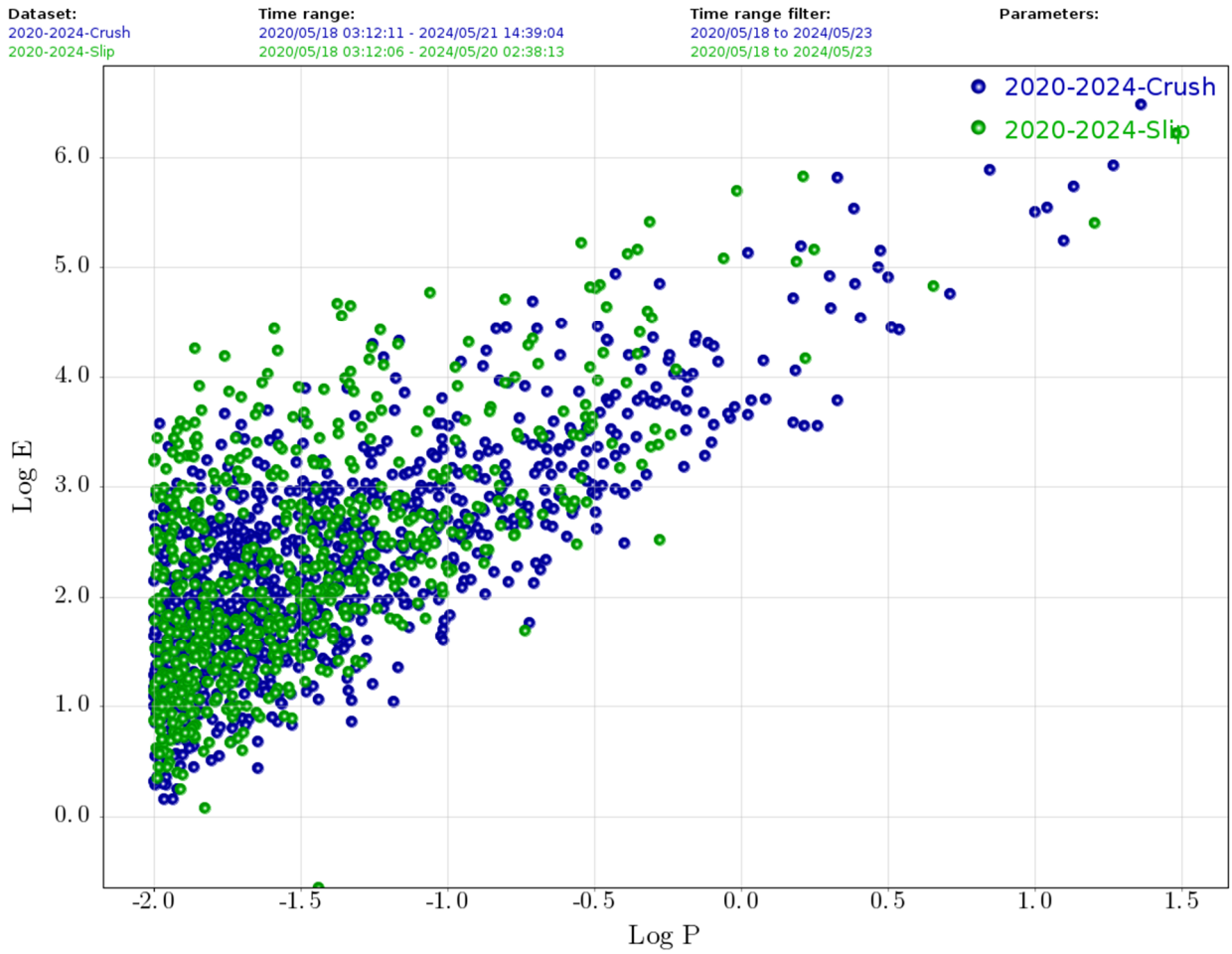

Figure 9 LogE-LogP plot for slip- and crush-type events in the area of interest since the May 2020 large event. Only events with logP > –2.0 are shown as below this, energy estimates become more scattered. Slip-type events are seen to have a larger energy range, while crush-type events tend to have a fairly well-defined narrow energy range. On average, slip events would have a higher energy index

Figure 10 illustrates the time history of slip and crush events and cumulative potency (with LogP > –2.0) since the large event. In terms of number of events, both were initially being recorded at a similar rate following the large event, although the cumulative potency shows that there was more crush-type deformation during this period. In early 2022 there was a strong increase in the number of crush events and a slight increase in the number of slip events. This corresponds to a period when hydraulic fracturing was done in the area, which induced an increase in small events of both slip- and crush-type. It is worth noting that although the number of events here was extremely high, the cumulative potency change did not increase dramatically, which shows it is still rather dictated by other sporadic larger events. The cumulative potency from slip-type events had a few notable steps around early 2023, otherwise remaining low and flat.

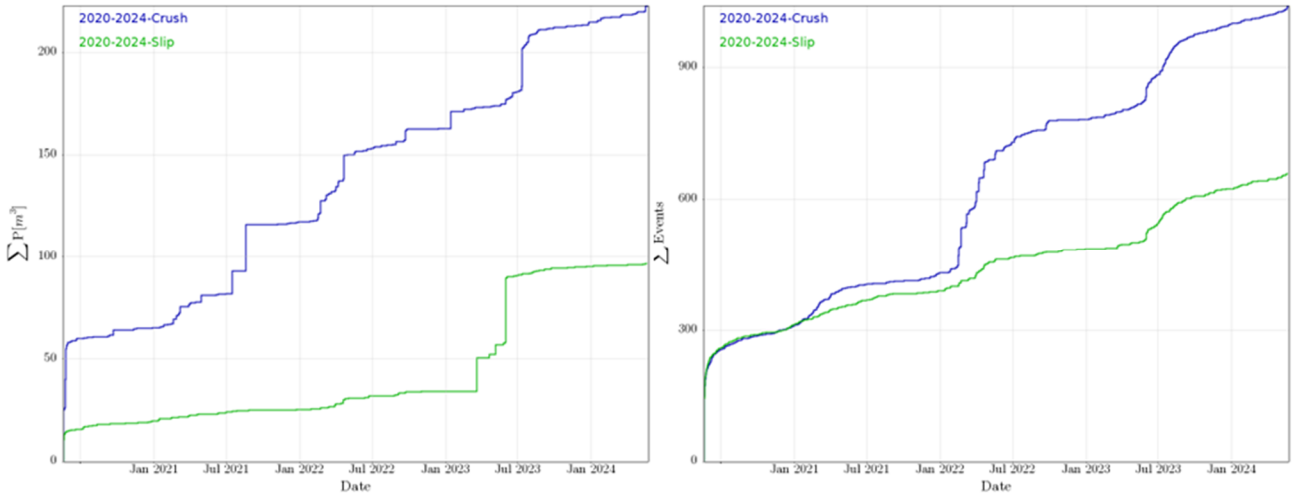

Figure 10 Time history of the cumulative number of events (left) and cumulative potency (right) of slip-type and crush-type events with LogP > –2.0

3 Examples of seismically induced falls of ground

Since May 2020 there have been several cases of seismically induced falls of ground at Kiruna mine. This section contains two examples in different parts of the mine and the associated mechanisms.

3.1 15 January 2024

On 15 January 2024 a ML0.8 (MW1.0) strainburst occurred on the 1108 level in Block 15. Photos of the damage are shown in Figure 11, along with the processed event location and source mechanism; the solution of which is shown in Figures 11 and 12. The best inverted source mechanism is predominantly crush-type and the P-axis is orthogonal to the strike of the excavation, dipping to the east. The source mechanism confidence plots are shown in Figure 13.

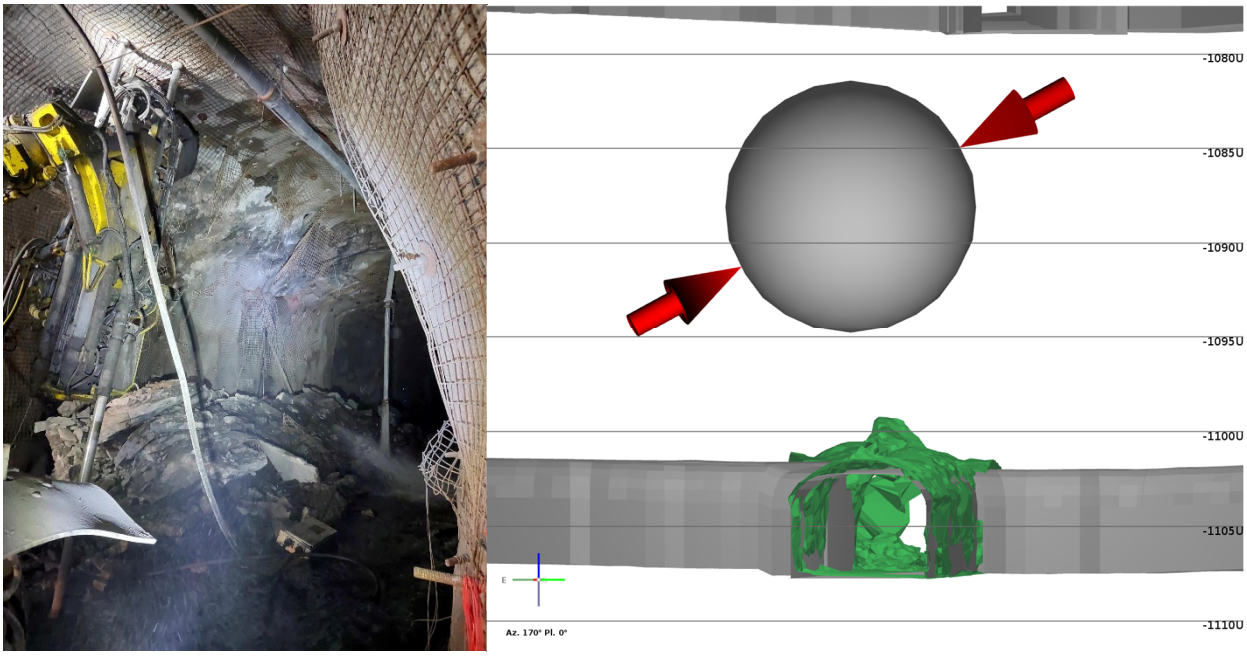

(a) (b)

Figure 11 (a) Photo of damage; (b) Processed event location and source mechanism relative to damage (green scans)

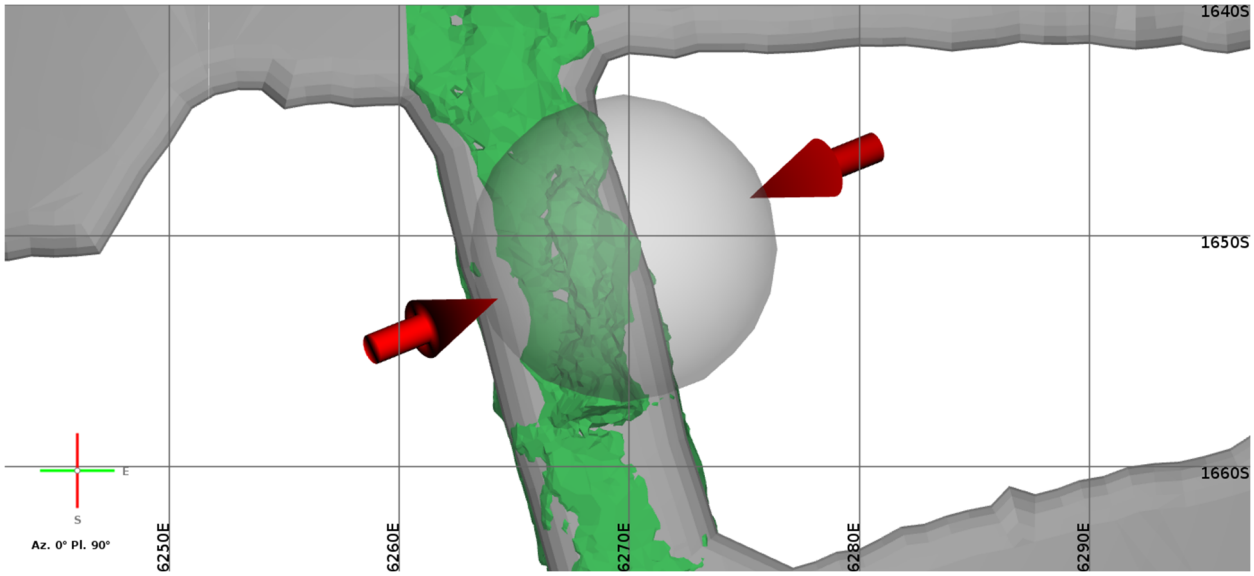

Figure 12 Plan view of the source mechanism above the damaged area

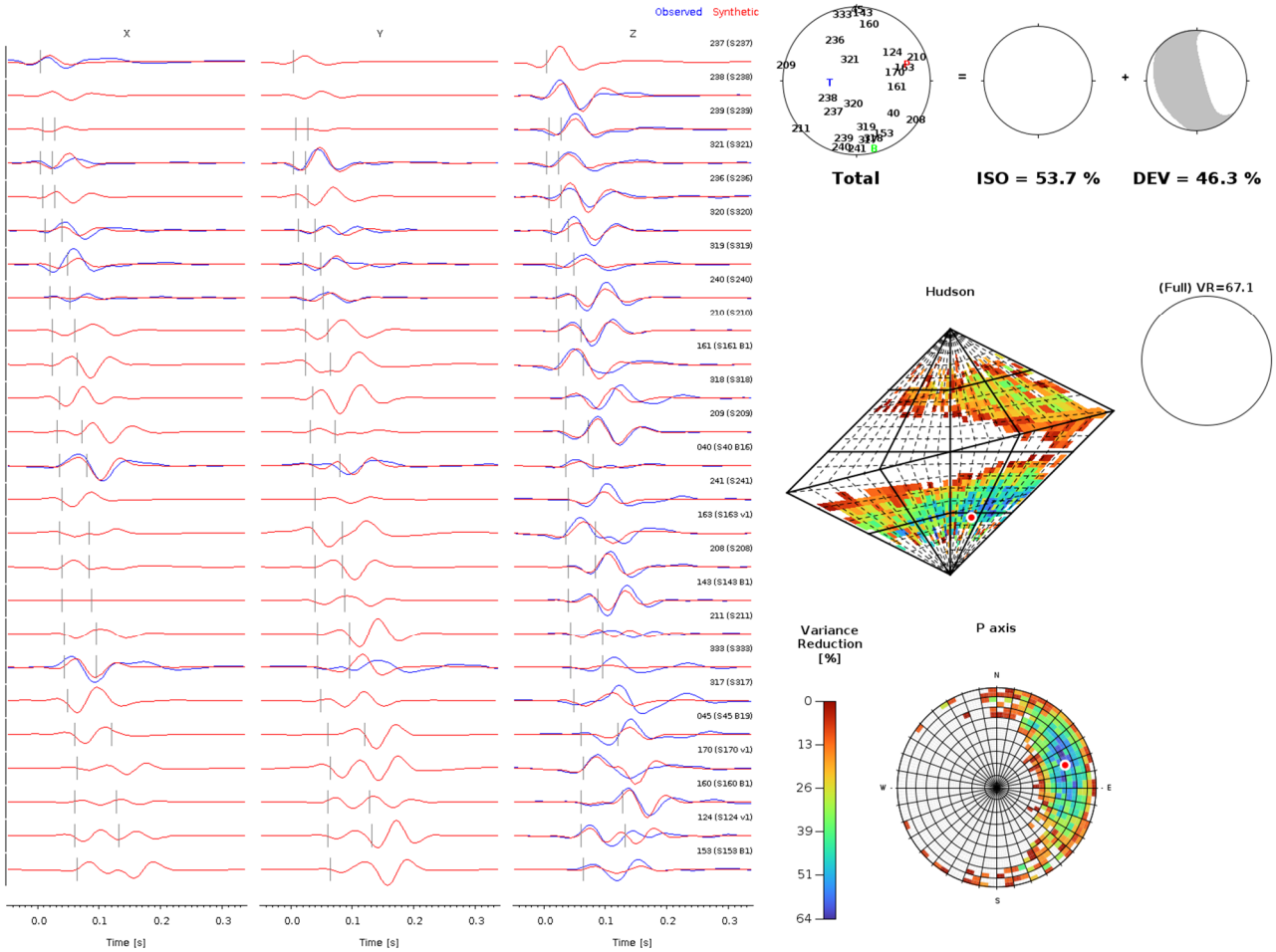

Figure 13 Source mechanism confidence plots. The focal sphere is well covered and the confidence in the solution is good

Using the model described in Malovichko & Rigby (2022), one can estimate the seismic moment (and hence moment magnitude) of a crush-type event based on the physical dimensions of the burst (linear extent, depth of failure), the rock mass properties and the maximum in-plane stress (see Equation 1).

$$|M| \approx 2\frac{1-\nu}{1-2\nu}|\sigma_{max}|L_3\overline{L_A}\Delta d_f^A \quad (1)$$

where:

ν = Poisson's ratio

σ_{max} = maximum stress in the plane orthogonal to the excavation

L_3 = extent of damage along the tunnel

L_A = effective tunnel dimension

Δd_f^A = increase in the depth of failure.

From the scans, L_3 was estimated at 10 m. The depth of failure increase varied from around 1.5 to 2.5 m, a value of 2 m. Numerical modelling of the area shows that σ_{max} is likely to be approximately 55 MPa and ν was 0.27 (estimated from seismic data).

With these assumed values, the moment magnitude associated with the increase in the depth of failure is around 0.86. Traditional estimates based on spectra analysis found MW1.0. The values are therefore in agreement, with the small difference being based on uncertainties in the values assigned in Equation 1 or due to the fact that there may be parts of the seismic radiation that were from minor shearing part of the event. There was some evidence of this in the source-type solution (Hudson plot in Figure 13), which shows that the event does have some double couple (DC) component; a pure crush event with no DC would be closer to the lower right boundary of the plot.

The seismic source mechanism inversion allows us to estimate the duration of the bulking process based on the time difference between the origin time of the event (based on first arrivals, when failure was initiated) and the moment tensor centroid time (time of maximum displacement). In this case the difference was found to be 40 ms. Using the model of Moss & Kaiser (2022) to combine this duration with the depth of failure allows us to estimate the velocity and subsequent energy demand placed on the ground support during the strainburst. One unknown is the bulking factor, which for now we assume to be 6%. A 2 m depth of failure with 6% bulking factor would impose a displacement demand of 120 mm. If this happened over the course of 40 ms, the velocity of the material at the skin of the excavation due to bulking behind it would be 3 m/s. Assuming a rock mass density of 2,800 kg/m^3, this indicates an energy demand of 3.15 kJ/m^2.

3.2 7 February 2024

Figure 14 shows damage from an ML1.9 (MW2.1) event in Block 41. This area is at the edge of the mine and has poorer 3D sensor coverage than the previously shown event due to the limited access available to install seismic sensors. However, a seismic source mechanism inversion is still possible, with the results shown in Figure 15.

Multiple support failure mechanisms were observed, including shear, tensile failure, pull-out failure and failure of surface support elements such as bolt plates. Corrosion was a factor that contributed to reduced support capacity in this area.

Figure 14 View of the damage from the event after some rock had been removed, looking south

The resultant seismic source mechanism is a mix of crush and slip. The confidence plot indicates that the solution is less well constrained; likely due to the poorer coverage as shown in Figure 15.

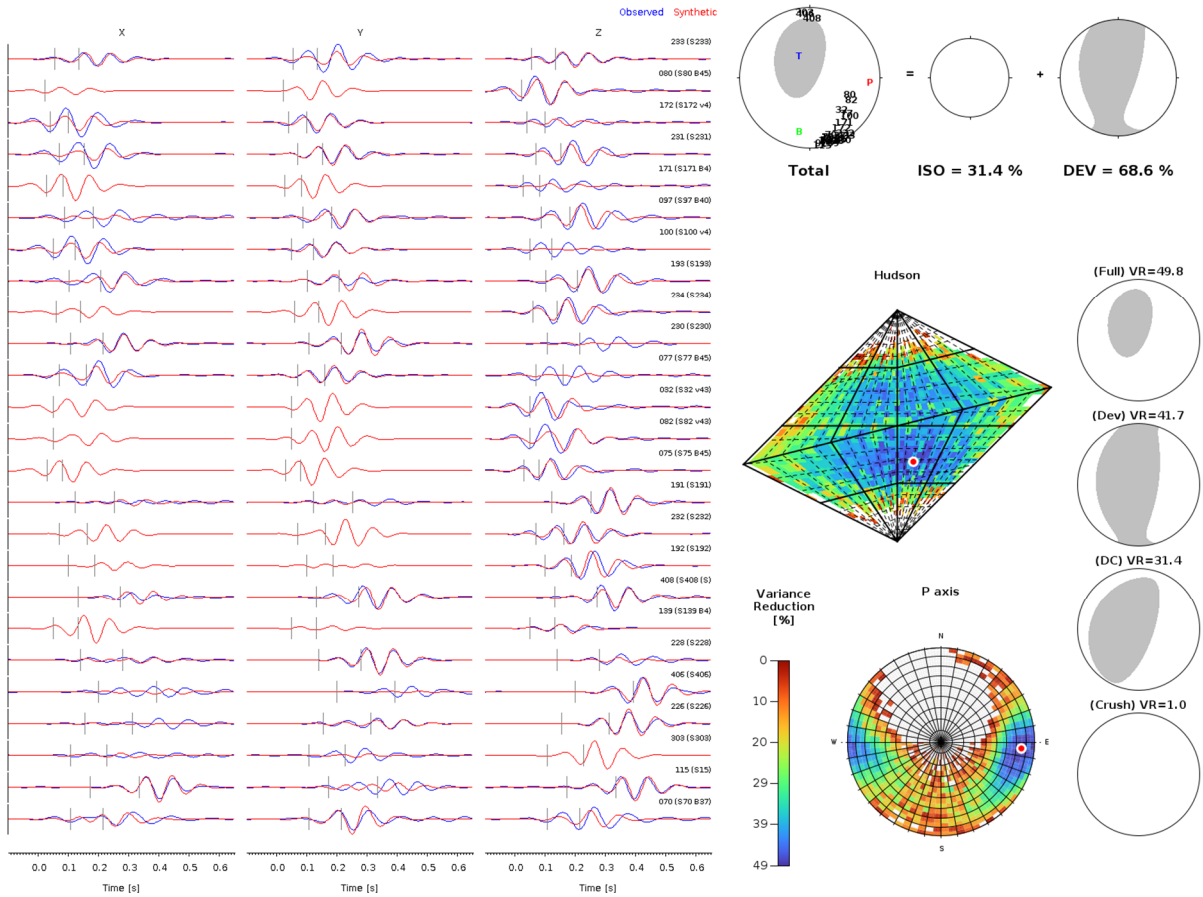

Figure 15 Quite good agreement between the observed and synthetic waveforms was found. The confidence plots are, however, not as well constrained

The seismic source mechanism inversion process provided a source duration of 57 ms. However, the fact that the source mechanism is poorly constrained and has a best solution corresponding to a combined slip and crush event implies that adopting this as the bulking duration may not be appropriate, especially as there is also evidence of shear deformation. This is further backed up by waveform observation which shows multiple pairs of phase arrivals (Figure 16), indicating a complex source for which some of the approximations may not be valid. For example, the relatively long source duration may be related to multiple, distinct episodes of failure along the extent of the excavation rather than the actual radial evolution of the bursting and bulking process.

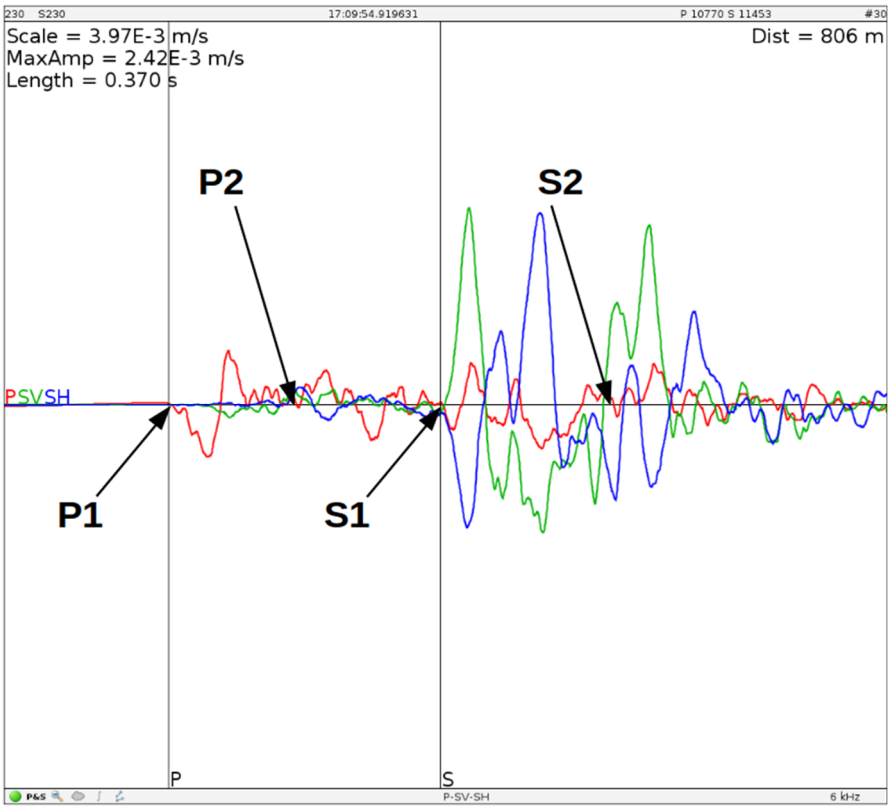

Figure 16 Example waveform from the MW2.1 event on 7 February 2024. The waveforms are somewhat complex, with evidence of a later arrival (P2, S2) about 60 ms after the initial (P1, S1)

In such a case, the complex waveforms and lower confidence may cast doubt when applying the methods used for the previous event. This event may first require further study through other techniques such as finite source inversion, similarly to the May 2020 event, which has not been completed yet. This may provide a more reasonable description of the source which can then be studied in terms of the dynamic loading. However, the poorer 3D coverage may limit the success of this approach.

4 Implications for mine design and operations

The above examples illustrate how data quality is key to the applicability of moment tensor decompositions in assisting with interpretation of rock mass failure mechanisms.

To account for Kiruna's increasing depth, numerous measures have been taken to reduce the seismic risk to underground operations. This includes evaluations of and updates to the mine's blasting protocols, exclusion zones, seismic risk management plan and trigger action response plans, and other tools and methods used to reduce risk and exposure in a seismically active mine.

Currently Kiruna mine is using chevron-shaped vertical mining sequencing (Figure 17).

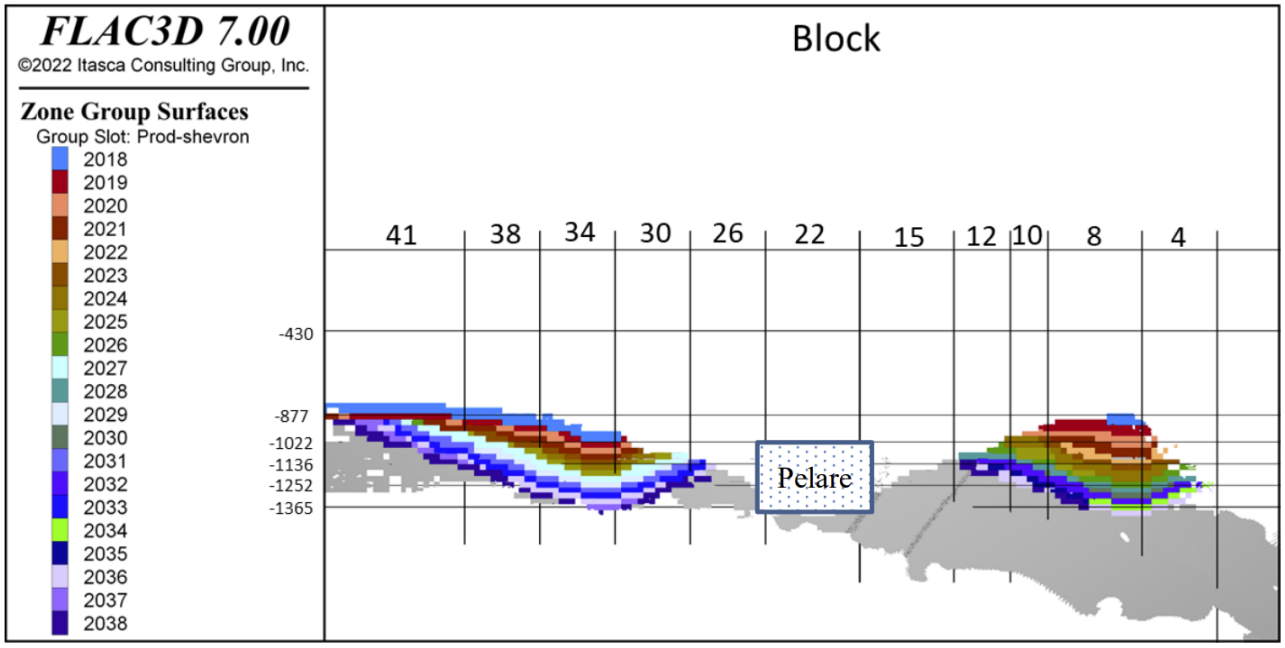

Figure 17 Example of a chevron sequence (Rentzelos et al. 2024)

Work is in progress to separate the mine into decoupled production areas to be managed according to risk, value, orebody geometry (as shown in Figure 18) and other factors to improve flexibility, assure reliable production and prevent large-scale interaction across large mining fronts when possible.

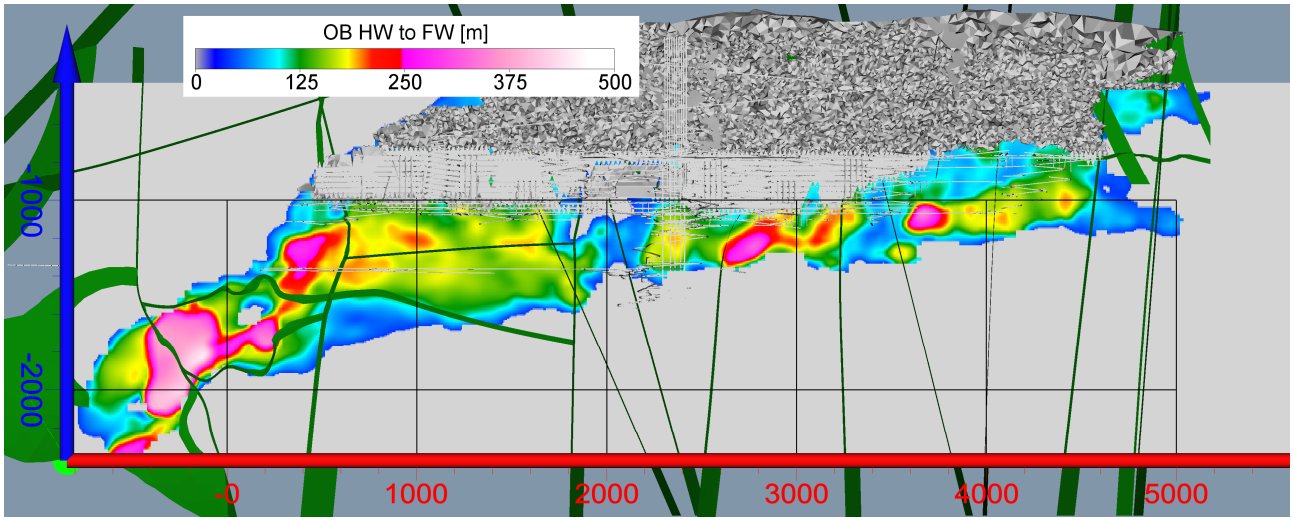

Figure 18 Orebody thickness from hanging wall to footwall (Beck et al. 2024)

Based on natural variation in orebody thickness, this could be considered with other factors to divide the mine into more than the two current production zones.

5 Conclusion

An overview of the seismicity at Kiruna mine since the 18 May 2020 event shows that both slip- and crush-type events are responsible for ongoing activity in the sector that was most affected by the large event.

Moment tensor decompositions of events relating to falls of ground generally show that crush-type events are a component of ground failures similar to that which occurred in the January 2024 event, while larger events resulting in failures tend to have complex mechanisms and waveforms, as experienced in the 7 February 2024 event.

Kiruna mine is re-evaluating the sequencing approach so as to avoid large volumes of high stress concentrations, and decoupling the mine into independent production zones.

Acknowledgement

The authors would like to acknowledge KGE (Kiruna Rock Mechanics) and KGG (Kiruna Mine Planning and Geology), Matthias Wimmer (LKAB), Joel Kangas (LKAB), Dmitriy Malovichko (Institute of Mine Seismology), Peter Kaiser (GeoK) and David Beck (Beck Engineering) for their support related to this work.

References

Allen, R 2021, *Geological Interpretation of LKAB Per Geijer Drill Holes 20 0024 and 21 001*, LKAB Investigation, no. 2021-0033.

Andersson, JBH, Bauer, TE & Martinsson, O 2021, 'Structural evolution of the central Kiruna Area, Northern Norrbotten, Sweden: implications on the geologic setting generating iron oxide-apatite and epigenetic iron and copper sulfides', *Economic Geology*, vol. 116, pp. 1981–2009.

Andersson, UB 2023, *Compilation and Evaluation of Uniaxial Compressive Strength Tests of Rocks from Kiirunavaara*, LKAB, Kiruna.

Andersson, UB, Samuelsson, E, Israelsson, J, Mattsson, K-J, Winell, S, Stråhle, A & Carlsten, S 2012, *Boremapkartering och Geologisk Beskrivning av Kiruna Underjordsverkstad (KUV), nivå 1365, Kiirunavaar*a, LKAB Investigation, no. 12-797, pp. 1–34.

Beck, D, Kusui, A & Dehkoda, S 2024, *Kiruna Below -1365mRL Part 1 Draft*, report.

Bergman, S, Kübler, L & Martinsson, O 2001, 'Description of regional geological and geophysical maps of northern Norrbotten county (east of the Caledonian orogen)', *Sveriges Geologiska Undersökning*, Ba 56, Geological Survey of Sweden, Uppsala.

Dineva, S & Boskovic, M 2017, 'Evolution of seismicity at Kiruna Mine', in J Wesseloo (ed.), *Deep Mining 2017: Proceedings of the Eighth International Conference on Deep and High Stress Mining*, Australian Centre for Geomechanics, Perth, pp. 125–139, https://doi.org/10.36487/ACG_rep/1704_07_Dineva

Geijer, P 1910, 'Igneous rocks and iron ores of Kiirunavaara, Luossavaara and Tuollavaara', *Scientific and Practical Research in Lapland Arranged by the Luossavaara-Kiirunavaara Aktiebolag, Geology of the Kiruna district*, vol. 2, Stockholm, pp. 1–278.

Heal, D, Potvin, Y & Hudyma, M 2006, 'Evaluating rockburst damage potential in underground mining', *Proceedings of Golden Rocks 2006: The 41st US Symposium on Rock Mechanics: 50 Years of Rock Mechanics - Landmarks and Future Challenges*, American Rock Mechanics Association, Alexandria.

Kaiser, PK, Tannant, DD, McCreath, DR & Jesenak, P 1992, 'Rockburst damage assessment procedure', *Proceedings of the International Symposium on Rock Support*, A.A. Balkema, Rotterdam, pp. 639–647.

Lindberg, A 2023, 'Europe's largest deposit of rare earth metals is located in the Kiruna area', *LKAB Press Release*, viewed 2 June 2024, https://mb.cision.com/Main/11419/3696865/1777621.pdf

Malovichko, D & Rigby, A 2022, 'Description of seismic sources in underground mines: dynamic stress fracturing around tunnels and strainbursting', *arXiv*, https://arxiv.org/abs/2205.07379

Martinsson, O 2004, 'Geology and metallogeny of the northern Norrbotten Fe-Cu-Au province', *Svecofennian Ore-Forming Environments Field Trip Volcanic-Associated Zn-Cu-Au-Ag and Magnetite-Apatite, Sediment Hosted Pb-Zn, and Intrusion-Associated Cu-Au Deposits in Northern Sweden, SEG Guidebook Series*, vol. 33, Society of Economic Geologists, Littleton, pp. 131–148.

McGurk, T, Baker, H & Dishaw, G 2023, *A Competent Persons Report on the Mineral Resources and Mineral Reserves of LKAB, Sweden - Kiruna Mine*, *LKAB*, Kiruna.

Moss, A & Kaiser, PK 2022, 'An operational approach to ground control in deep mines', *Journal of Rock Mechanics and Geotechnical Engineering*, vol. 14, no. 1, pp. 67–81.

Rentzelos, T, Andersson, J, Swindell, R & Perman, F 2024, *Optimization of Barrier Pillar Geometry and Evaluation of Alternative Mining Sequences for the Kiirunavaara Mine*, LKAB internal report.

Sandström, D 2003, *Analysis of the Virgin State of Stress at the Kiirunavaara Mine*, licentiate thesis, Luleå University of Technology, Luleå.

Sjöberg, J, Lundman, P & Nordlund, E 2001, 'Analys och prognos av utfall i bergschakt, KUJ 1045 slutrapport', LKAB Investigation, no. 01-762, internal report, LKAB, Kiruna.

Swedberg, E 2022, *Block 22 – Damage Mapping Summary*, LKAB internal presentation.

Westhues, A, Hanchar, JM, Whitehouse, MJ & Martinsson, O 2016, 'New constraints on the timing of host rock emplacement, hydrothermal alteration, and iron oxide-apatite mineralization in the Kiruna district, Norrbotten, Sweden', *Economic Geology*, vol. 111, no. 7, pp. 1595–1618.

Ylmefors, A 2023, *Classification of Mining Induced Seismicity at the Kiirunavaara Mine*, PhD thesis, Luleå University of Technology, Luleå.